iScience

CellPress
OPEN ACCESS

Article

Splicing factor Srsf5 deletion disrupts alternative splicing and causes noncompaction of ventricular myocardium

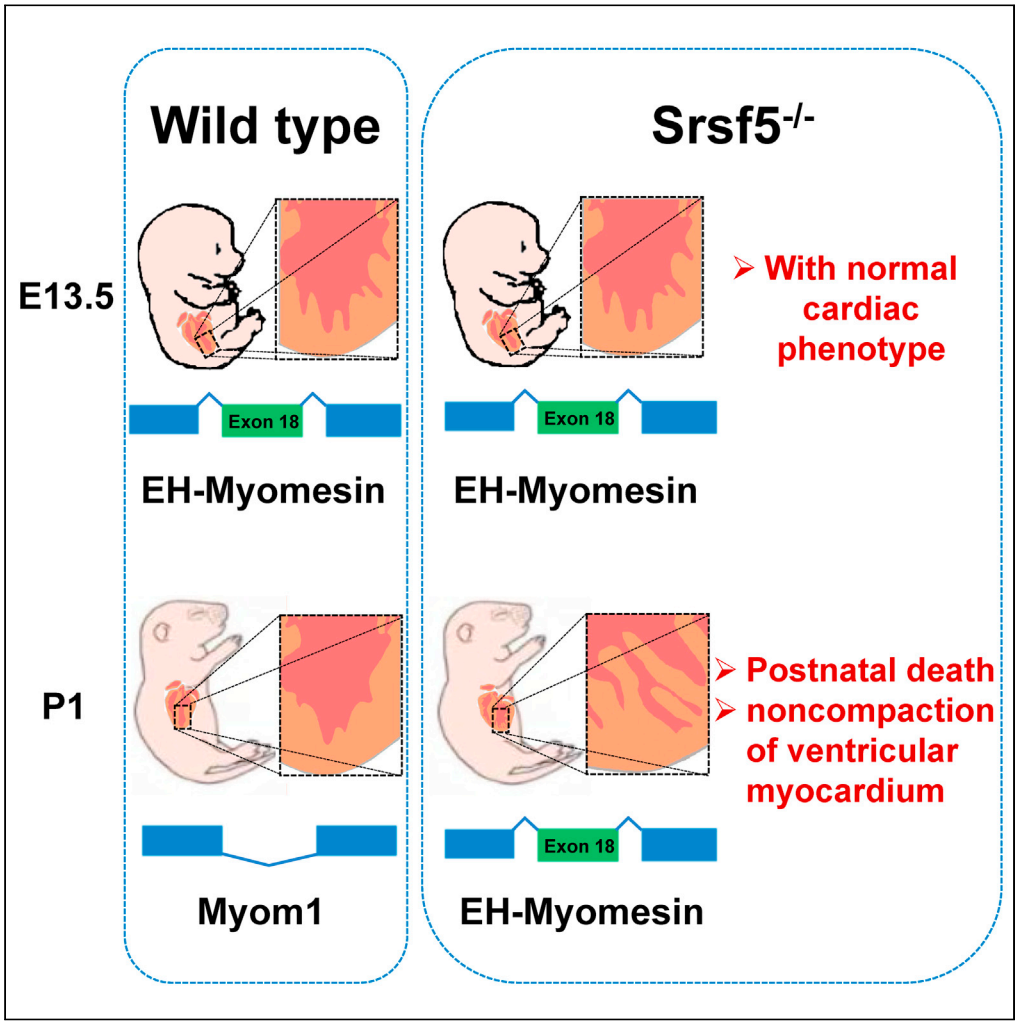

Xiaoli Zhang, Ze Wang, Qing Xu, ..., Chengshi Quan, Lingqiang Zhang, Chun-Ping Cui

cui_chunping2000@aliyun.com (C.-P.C.)
zhanglq@nic.bmi.ac.cn (L.Z.)
quancs@jlu.edu.cn (C.Q.)

Highlights

Systemic loss of Srsf5 causes perinatal lethality in mice

Srsf5 deficiency leads to cardiac dysfunction

Alternative splicing of Myom1 in the heart around birth is regulated by Srsf5

Zhang et al., iScience 24, 103097
October 22, 2021
https://doi.org/10.1016/j.isci.2021.103097

iScience

CellPress
OPEN ACCESS

Article

Splicing factor Srsf5 deletion disrupts alternative splicing and causes noncompaction of ventricular myocardium

Xiaoli Zhang,[1,2] Ze Wang,[2] Qing Xu,[3] Yuhan Chen,[2] Wen Liu,[2] Tong Zhong,[2] Hongchang Li,[2] Chengshi Quan,[1,*] Lingqiang Zhang,[2,*] and Chun-Ping Cui[2,4,*]

SUMMARY

The serine/arginine-rich (SR) family of splicing factors plays important roles in mRNA splicing activation, repression, export, stabilization, and translation. SR-splicing factor 5 (SRSF5) is a glucose-inducible protein that promotes tumor cell growth. However, the functional role of SRSF5 in tissue development and disease remains unknown. Here, *Srsf5* knockout (*Srsf5*$^{-/-}$) mice were generated using CRISPR-Cas9. Mutant mice were perinatally lethal and exhibited cardiac dysfunction with noncompaction of the ventricular myocardium. The left ventricular internal diameter and volume were increased in *Srsf5*$^{-/-}$ mice during systole. Null mice had abnormal electrocardiogram patterns, indicative of a light atrioventricular block. Mechanistically, Srsf5 promoted the alternative splicing of Myom1 (myomesin-1), a protein that crosslinks myosin filaments to the sarcomeric M-line. The switch between embryonic and adult isoforms of Myom1 could not be completed in *Srsf5*-deficient heart. These findings indicate that Srsf5-regulated alternative splicing plays a critical role during heart development.

INTRODUCTION

Precursor messenger RNA (pre-mRNA) undergoes various splicing reactions to form mature mRNAs (Crick, 1979; Sharp, 1994). The alternative splicing of pre-mRNA allows eukaryotic cells to produce a wide variety of proteins from a limited number of genes. Current transcriptomic sequencing and high-resolution mass spectrometry analyses suggest that almost all human genes occur in alternative splicing events (Barbosa-Morais et al., 2012; Merkin et al., 2012), and 37% of the genes encoding proteins generate diverse protein isoforms (Kim et al., 2014). Alternative splicing plays an important physiological function during tissue and organ development; distinct cell types form unique splicing regulatory networks, and faulty splicing causes severe developmental defects (Baralle and Giudice, 2017).

Alternative splicing is executed by the spliceosome complex, which consists of five small nuclear ribonucleoprotein particles (U1, U2, U4/U6, and U5) (Shi, 2017) and is regulated by multiple non-spliceosomal RNA-binding proteins, including serine and arginine-rich (SR) proteins, heterogeneous nuclear ribonucleoprotein particles (hnRNPs), and other RNA-binding proteins (RBPs) (Lee and Rio, 2015). SR-splicing factors (SRSFs) generally promote splicing at adjacent sites whereas hnRNPs antagonize the positive effects of SRSFs and repress splicing (Geuens et al., 2016). However, the regulation of alternative splicing by SRSF is more complicated. The location where SRSFs interact with RNA influences their activated or repressive function, and SRSFs activate or inhibit other RBPs in a context-dependent manner (Fu and Ares, 2014; Zhou and Fu, 2013).

To date, all reported classical *Srsf*-knockout mice display an early embryonic lethal phenotype. Mice with a cardiac conditional deletion of *Srsf1* die several months after birth, and their hearts display a hypercontraction phenotype due to the inability of Ca^{2+} handling protein CaMKIIδ to complete the postnatal splice isoform transition (Xu et al., 2005). Srsf2 inactivation in the thymus results in defective T cell maturation due to the incorrect alternative splicing of *CD45* exon 5 (Wang et al., 2001). Loss of Srsf2 in the liver causes liver failure and death in mice within four weeks of birth. Srsf2 acts as a splicing factor to regulate cell death transcriptional events and as a transcriptional activator to regulate the transcription of genes related to liver metabolism (Cheng et al., 2016). The systemic knockout of *Srsf10* results in defective cardiac development

[1]The Key Laboratory of Pathobiology, Ministry of Education, College of Basic Medical Sciences, Jilin University, 126 Xinmin Avenue, Changchun, Jilin 130021, China

[2]State Key Laboratory of Proteomics, Beijing Proteome Research Center, National Center for Protein Sciences (Beijing), Beijing Institute of Lifeomics, 27 Taiping Road, Beijing 100850, China

[3]Core Facilities Centre, Capital Medical University, Beijing 100069, China

[4]Lead contact

*Correspondence: cui_chunping2000@aliyun.com (C.-P.C.), zhanglq@nic.bmi.ac.cn (L.Z.), quancs@jlu.edu.cn (C.Q.)

https://doi.org/10.1016/j.isci.2021.103097

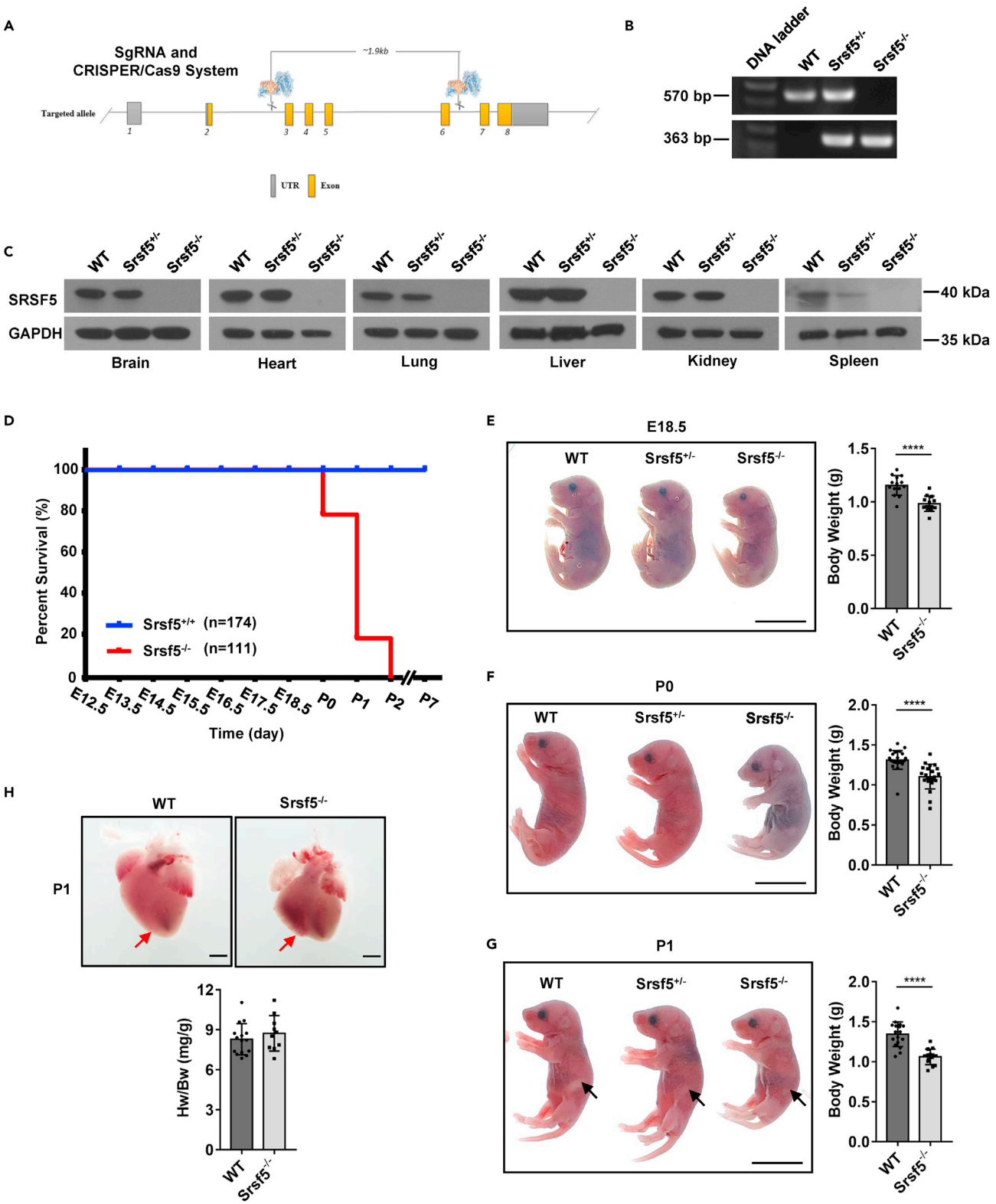

Figure 1. *Srsf5* knockout causes perinatal lethality in mice

(A) Gene-targeting strategy for the *Srsf5* gene. The gRNA direct Cas9 endonuclease cleavage of *Srsf5* gene and creation of a DSB (double-strand break). DSBs were repaired by non-homologous end-joining (NHEJ), resulting in the deletion of exon 3–6.

Figure 1. *Continued*

(B) Genomic DNA was extracted from tails and analyzed by PCR to detect the genotype.

(C)Western blot assay was used to examine Srsf5 protein level in the tissues of WT, *Srsf5*$^{+/-}$, and *Srsf5*$^{-/-}$ mice at E18.5.

(D) The Kaplan-Meier survival analysis was performed to show the lifespan of *Srsf5*$^{-/-}$ mice. There was a significant difference in survival between mutant mice and WT littermates ($p < 0.0001$ by logrank test).

(E–G) Gross morphology and body weight of WT and *Srsf5*$^{-/-}$ pups at E18.5 (E), P0 (F), and P1 (G). Null mice were much smaller, and living P1 pups were pale and had no food in their stomachs. The black arrow indicates the stomach. Scale bar, 10 mm.

(H) Gross morphology and heart weight (Hw) to body weight (Bw) ratio in the hearts of WT and *Srsf5*$^{-/-}$ mice at P1. The red arrow indicates an abnormality of the right ventricular apex. Scale bar, 1 mm. Data are represented as mean ± SD. ****: $p < 0.0001$, Student's t-test.

See also Figure S1.

and the abnormal splicing of calcium-regulated gene *triadin*, which gives rise to defective calcium handling in cardiomyocytes (Feng et al., 2009). The absence of Srsf3 in the heart of both embryonic and adult mice results in death. Srsf3 deletion promotes the retention of mTOR intron 5, allowing mTOR to express a shorter isoform because of the stop codon in the intron, resulting in the inability of 4E-BP1 to be phosphorylated, as well as increased mRNA decapping (Ortiz-Sánchez et al., 2019). These results suggest that SR proteins are essential for tissue development and function maintenance. However, current studies are limited, and numerous roles of SRSFs remain to be discovered.

SRSF5 (also called SRp40 or SFRS5) contains the classical structure of the SR protein–one RNA recognition motif (RRM) domain, one RRM homology domain, and one RS domain (Shepard and Hertel, 2009). SRSF5 regulates mRNA splicing, such as exon skipping (Buratti et al., 2007; Sebbag-Sznajder et al., 2012) and exon inclusion (Du et al., 1997; Lu et al., 2013; Patel et al., 2005), the export of mRNA (Botti et al., 2017), and the stability of mRNA (Wu et al., 2020). In skeletal muscle cells, insulin activates the PI3K-AKT pathway to activate SRSF5 through direct phosphorylation via AKT2 kinase, which promotes PKCβII exon inclusion and the production of mature PKCβII mRNA, increasing glucose transport activity, and ensuring skeletal muscle energy metabolism (Patel et al., 2005). In the regenerating liver, SRSF5 was recognized as an insulin-inducible protein, regulating the alternative splicing of fibronectin by mediating EIIIB exon inclusion (Diamond et al., 1993; Du et al., 1997). We previously reported that SRSF5 is highly expressed as an oncogene in lung cancer. SRSF5 responds to high glucose levels in cancer cells, becomes more stable after acetylation, and promotes CCAR1 exon skipping to produce short isoforms, which promote tumor growth by enhancing glucose consumption and acetyl-CoA production (Chen et al., 2018). However, the functional role of SRSF5 in tissue development remains unknown.

In the present study, we generated *Srsf5*-deficient mice and found that mutant mice were perinatally lethal and exhibited cardiac dysfunction with noncompaction of the ventricular myocardium. Mechanistically, we observed that Srsf5 promoted the alterative splicing of Myom1, a protein that crosslinks myosin filaments to the sarcomeric M-line and maintains structural integrity during contraction. The switch between embryonic and adult isoform of Myom1 could not be completed in *Srsf5*-deficient cardiac, and more embryonic Myom1 isoforms were retained. Therefore, we conclude that Srsf5-regulated alternative splicing plays a critical role in heart development.

RESULTS

Srsf5-deficient mice display perinatal lethality

To evaluate the function of Srsf5, we generated *Srsf5* knockout (*Srsf5*$^{-/-}$) mice in which exons 3–6 of the *Srsf5* gene were cut using CRISPR/Cas9 technology (Figure 1A). The genotypes were confirmed by PCR analysis (Figure 1B). Western blot assay was used to confirm the complete deletion of Srsf5 protein in the *Srsf5*$^{-/-}$ tissues, compared with their wild-type (WT) littermates (Figure 1C). Heterozygous mice remained normal and fertile at six months of age. However, homozygous mice were not detected in the adult offspring of heterozygous crosses. The identification of embryo genotypes at various gestation periods revealed that all *Srsf5*$^{-/-}$ embryos were alive at developmental day 18.5 (E18.5) (observed 19.7% versus expected 25%, non-significant difference), but most died within 24 h of birth. No *Srsf5*$^{-/-}$ mice survived until postnatal day 2 (P2) (Figure 1D and Table 1).

Next, we examined the morphological properties of *Srsf5*$^{-/-}$ mice. The mutant mice were developmentally delayed and smaller than the littermate WT controls. The mice that died at P0 did not breathe at birth and were presumably born dead. Surviving mice at P1 were pale and had no milk in their stomachs (Figures1E–1G). Upon examination of tissues and organs, mice at P1 showed that the *Srsf5*$^{-/-}$ mice had an irregular

Table 1. Ratio of genotypes of offspring from *Srsf5*$^{+/-}$×*Srsf5*$^{+/-}$

Age	# Litters	# Pups	*Srsf5*$^{+/+}$	*Srsf5*$^{+/-}$	*Srsf5*$^{-/-}$
E18.5	20	157	46 (29.3)	80 (51.0)	31 (19.7)
P0	18	138	40 (29.0)	60 (43.5)	38 (27.5)/14* (10.1)
P1	13	97	27 (27.8)	47 (48.5)	23 (23.7)/20* (20.6)
P2	8	51	17 (33.3)	31 (60.8)	3 (5.9)/3* (5.9)
P7	13	78	24 (30.8)	54 (69.2)	0 (0)
Expected percentage (%)			25	50	25

*: found dead.

heart with a protruding right ventricular apex and a smaller spleen than the WT mice, while other organs appeared normal (Figures1H and S1A). Weight analysis demonstrated no significant difference in the heart-to-body weight ratio (Figure 1H).

We then examined the protein and mRNA expression of Srsf5 in P1 neonates using IHC and qRT-PCR assays. The results showed that Srsf5 was widely expressed in neonatal organs and was particularly high in the heart (FiguresS1B andS1C). To determine the temporal pattern of Srsf5 expression in the developing heart, we examined the Srsf5 protein levels in embryonic and postnatal hearts (from E13.5 to P60). The results revealed that Srsf5 was highly expressed at E13.5–E15.5, decreased gradually during later embryonic and postnatal stages, and was undetectable in adulthood (FiguresS1D andS1E). These data indicate that Srsf5 is highly activated in developing hearts, consistent with the fact that alternative splicing plays an essential role in cardiac development (van den Hoogenhof et al., 2016).

Systemic loss of Srsf5 results in cardiac dysfunction

Next, we investigated the function of the heart in *Srsf5*$^{-/-}$ mice. The echocardiographic assessment of conscious WT and *Srsf5*$^{-/-}$ mice at P1 revealed that *Srsf5*$^{-/-}$ mice exhibited reduced left ventricular systolic function (Figures2A and 2B). The left ventricular wall thickness was significantly thinner during diastole and systole in *Srsf5*$^{-/-}$ mice. The left ventricular internal diameter and left ventricular volume were increased in *Srsf5*$^{-/-}$ mice during systole. Thus, the ejection fraction and fraction shortening of mutant mice were reduced compared to those of WT mice (Figure 2B and Table S1). At the same age, null mice showed abnormal electrocardiogram patterns, with a QRS complex that was noticeably altered (Figure 2C). The QRS wave amplitude and heart rate were extremely low in the hearts of *Srsf5*$^{-/-}$ mice. Their PR and QT intervals were strikingly prolonged, implying a light atrioventricular block (Figure 2D and Table S2). Decreased cardiac function in *Srsf5*$^{-/-}$ mice was accompanied by abnormally high levels of brain natriuretic peptide (BNP) expression, a marker of myocardial injury, but no significant change in atrial natriuretic factor (ANF) expression (Figure 2E). Taken together, these findings indicate the essential function of Srsf5 in the wall motion of neonatal hearts.

Srsf5$^{-/-}$ mice exhibit noncompaction of ventricular myocardium

SRSF5 has been demonstrated to regulate the alternative splicing of fibronectin exon EIIIA, which is necessary for the progression of chondrogenesis (Kuo et al., 2002). However, no cartilage defects were observed in the *Srsf5*$^{-/-}$ mice (Figure S2A), which is consistent with previous reports, wherein the abundance of SRSF5 was not the single factor limiting exon EIIIA inclusion in cells of chondrocyte origin (Kuo et al., 2002). Histopathological analysis suggested that the intestine, lung, liver, kidney, spleen, and brain were all developed normally in *Srsf5*$^{-/-}$ mice (Figure S2B). H&E staining showed that at E18.5 and P1, the hearts of WT mice had a thick myocardial compact layer with short and few myocardial trabeculae (Figures3A and 3B). Although structurally intact with clearly visible valves, the hearts of mutant mice had thinner compacted myocardial layers in both ventricles and long and densely arranged myocardial trabeculae that formed a prominent trabecular meshwork. Visualization at a high magnification further revealed the widening of the subendocardial intermuscular space and the vacuolar degeneration of some cardiomyocytes in the hearts of *Srsf5*$^{-/-}$ mice (Figures3A and 3B). To quantify the degree of myocardial densification, endomucin and cTnT immunofluorescence staining was used to label the endocardial contour and myocardium, respectively, as previously described (D'Amato et al., 2016; Zou et al., 2018). As shown in Figures3C–3F, the compact layer of myocardium was visibly thinner and the reticular myocardial trabeculae were thicker in the mutant hearts than in the control. Defects in ventricular compaction have been implicated as a cause of congenital heart disease, with clinical manifestations ranging from asymptomatic to sudden cardiac

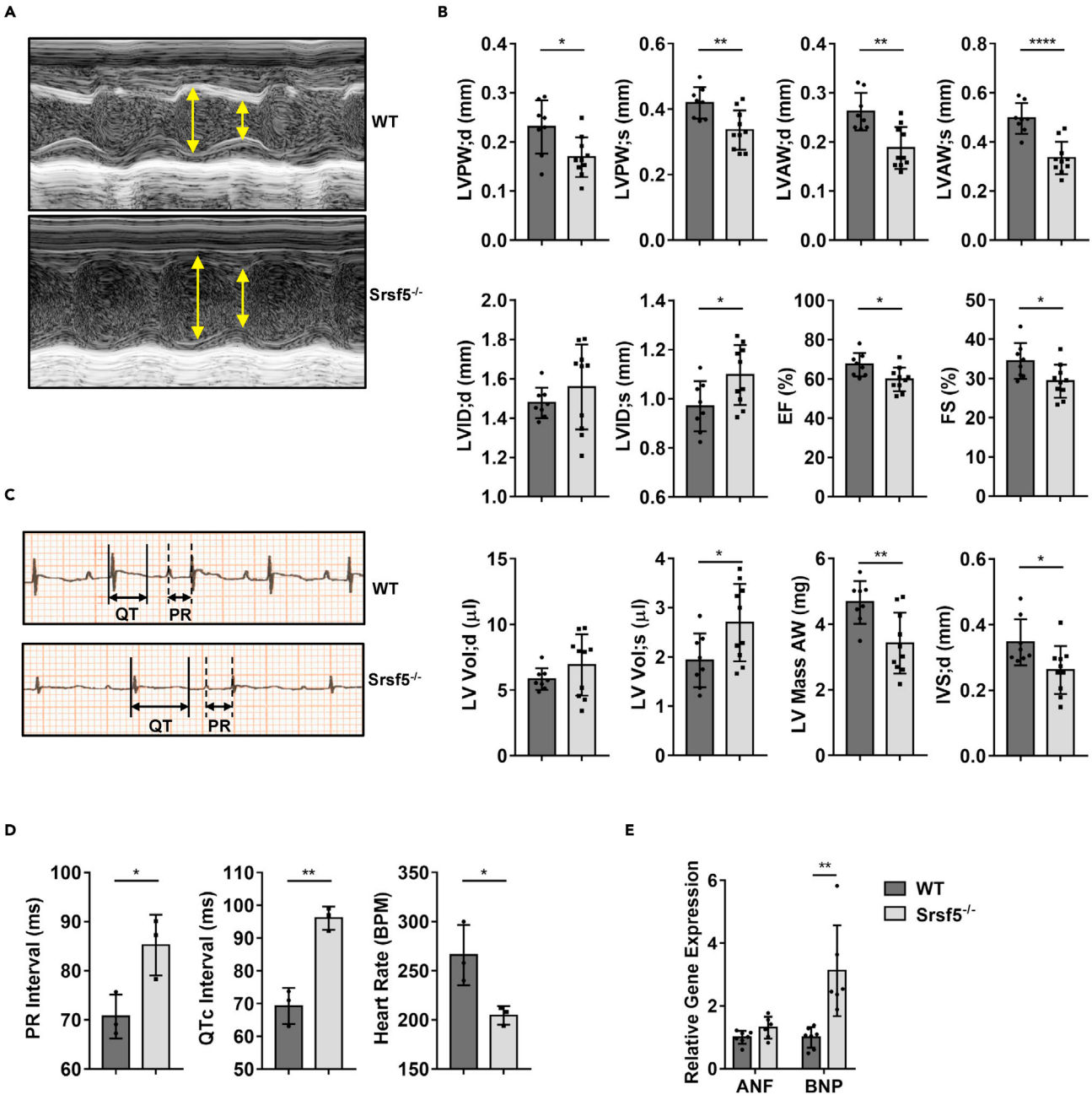

Figure 2. Cardiac contractile dysfunction and increased myocardial injury marker in the hearts of *Srsf5*$^{-/-}$mice

(A and B) Echocardiography was performed for all genotypes at P1. Representative M-mode pictures (A) and quantification of cardiac function indicators (B) are shown. The yellow arrow indicates the left ventricular (LV) internal diameter, and the long and short arrows indicate diastole (D) and systole (s), respectively. LVPWs, LV systolic posterior wall thickness; LVPWd, LV diastolic posterior wall thickness; LVAWs, LV systolic anterior wall thickness; LVAWd, LV diastolic anterior wall thickness; LVIDs, LV systolic internal dimension; LVIDd, LV diastolic internal dimension; EF, ejection fraction; FS, fractional shortening; IVSd, Interventricular septal thickness at diastole; Vol, Volume.

(C and D) Electrocardiographic analysis of WT and mutant mice at P1. Representative images (C) and the quantification of the PR interval, corrected QT (QTc) interval, and heart rate (D) are displayed.

(E) qRT-PCR analysis of heart failure markers in the hearts of P1 pups. Data are represented as mean ± SD. *: $p < 0.05$, **: $p < 0.01$, ****: $p < 0.0001$, Student's t-test. See also Tables S1 and S2.

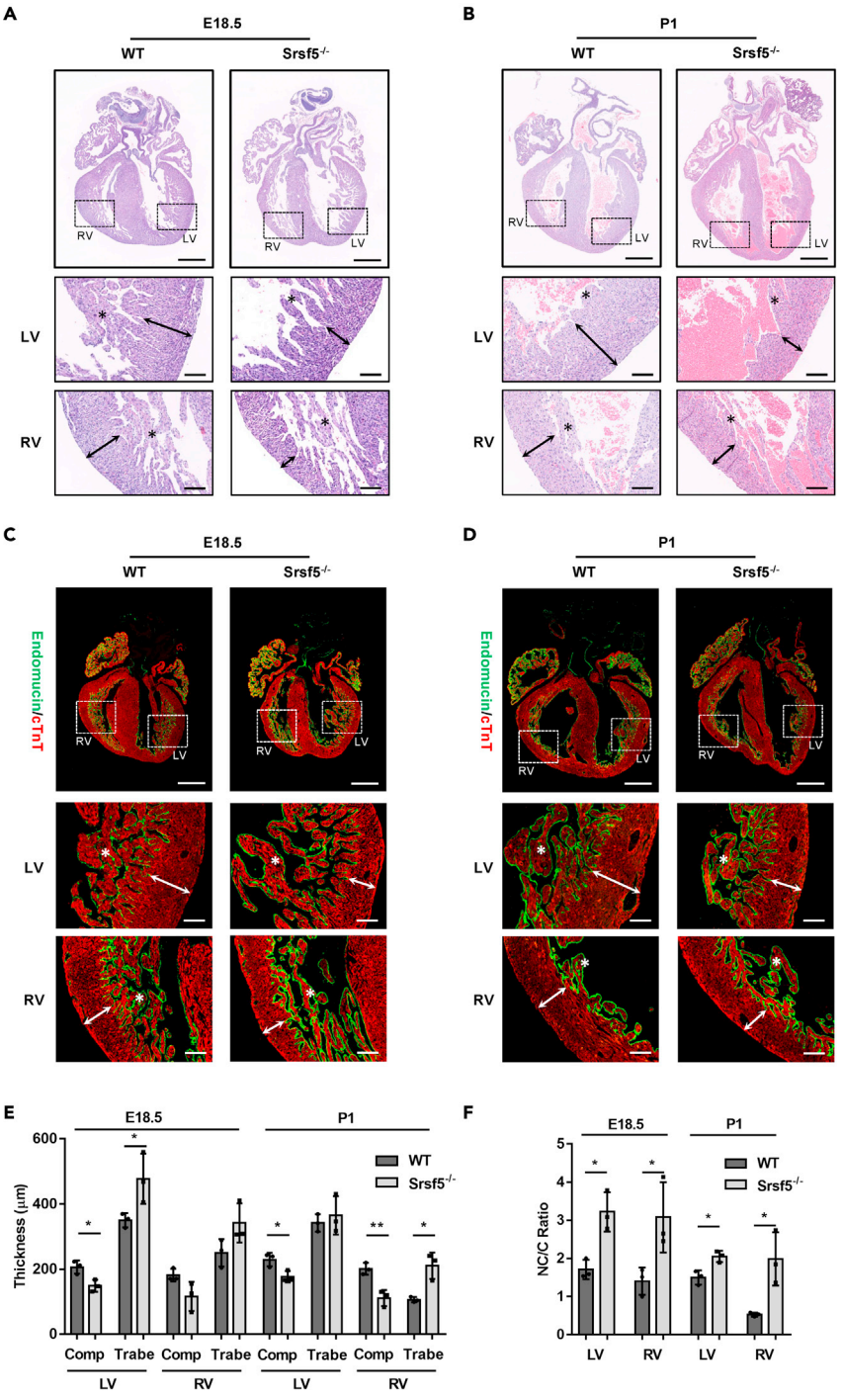

Figure 3. *Srsf5*$^{-/-}$ mice displays noncompaction of ventricular myocardium

(A and B) H&E staining of coronal sections of the heart of WT and *Srsf5*$^{-/-}$ mice at E18.5 (A) and P1 (B). The underside shows a magnified view of the dashed box-shaped area in the upper part. Arrows and asterisks indicate compact layer and myocardial trabecular thickness, respectively. Scale bar, 500 μm (top), 100 μm (middle and bottom).

(C and D) Immunofluorescence staining of E18.5 (C) and P1 (D) heart sections using endomucin (green) and cTnT (red) antibodies to represent the trabecular and compact layers. Scale bar, 500 μm (top), 100 μm (middle and bottom).

(E) Quantification of the thickness of the trabecular (Trabe) and compact (Comp) layers in the hearts of WT and *Srsf5*$^{-/-}$ mice.

Figure 3. *Continued*

(F) Analysis of the ratio of trabecular layer/compact layer thickness (NC/C ratio) in the hearts of WT and *Srsf5*$^{-/-}$ mice at E18.5 and P1. LV, left ventricular; RV, right ventricle. Data are represented as mean ± SD. *: p< 0.05, **: p< 0.01, Student's t-test.

See also Figure S2.

death (Ichida, 2020; Maron et al., 2006). Overall, these results indicate that Srsf5 deletion disrupts the normal structure of the heart and causes cardiomyopathy with noncompaction of the ventricular myocardium.

Embryonic heart growth depends mainly on the vigorous proliferation of cardiomyocytes (Galdos et al., 2017). The proliferation and growth of cardiomyocytes form the basis of trabecular formation and compaction. Gene regulation studies in mouse models have identified at least 60 genes that contribute to cardiomyocyte proliferation and growth, which play crucial roles in trabeculation and compaction (Wilsbacher and McNally, 2016). To determine whether Srsf5 plays an essential role in the growth of cardiomyocytes, we examined the expression of several proliferation-related factors in P1 hearts. Both Ki67 and pH3 IHC staining showed that the proliferation of cardiomyocytes was decreased in the hearts of *Srsf5*$^{-/-}$ mice (Figures4A–4D). The TUNEL assay showed no difference between the hearts of WT and mutant mice, suggesting that Srsf5 deletion did not influence the apoptosis of cardiomyocytes (Figures4E and 4F).

Identification of Srsf5-driven transcriptome and alternative splicing events in neonatal hearts

To elucidate the mechanism underlying the maintenance of myocardial contractile function by Srsf5, we performed RNA sequencing (RNA-Seq) in the hearts of WT and *Srsf5*$^{-/-}$ mice (n = 3) both at E18.5 and P0. To this end, we analyzed differential alternative splicing events and found that all five alternative splicing types were involved, including skipped exon (SE), retained intron (RI), mutually exclusive exons (MXE), alternative 5 splice site (A5SS), and alternative 3 splice site (A3SS) (Tables S4 and S5). Considering that more differential alternative splicing events occurred at P0 (P0: 583 events *vs.* E18.5: 162 events), we further analyzed the differential events from P0. Among them, SE (364 events) was the major differential alternative splicing type in the hearts of P0 *Srsf5* mutant *vs.* WT mice (Figure 5A). Figure 5B is the five-way Venn diagrams of the differential alternative splicing events, in which the number of alternative splicing genes were shown. This result illustrated a subset of overlapping genes between the five types of alternative splicing and suggested that different types of alternative splicing events occur in the same gene (Figure 5B). All genes in the alternative splicing events were subjected to gene ontology (GO) term enrichment analysis in DAVID. Notably, in GO terms related to biological processes, the genes were mainly annotated as those involved in sarcomere organization, muscle contraction, and heart morphogenesis (Figure 5C). Given that SRSF5 is an intermediate shuttler that facilitates the export of mRNA from the nucleus to the cytoplasm and maintains the stability of mRNA (Botti et al., 2017; Wu et al., 2020), we additionally analyzed the RNA-Seq data for differentially expressed genes. As demonstrated in the scatter plot, a total of 661 differentially expressed genes (DEGs) were identified in the hearts of P0 WT and *Srsf5*$^{-/-}$ mice (Figure 5D and Table S6). GO term enrichment analysis of DEGs revealed that myofibril was a highly affected cellular component (Figure 5E). Quantitative RT-PCR analysis was used to validate DEGs. The mRNA levels of *Mmp9*, *Mmp12*, and *Fgf16*, which promote cell proliferation (Dwivedi et al., 2009; Lavine et al., 2005), were significantly downregulated in the hearts of the mutant mice. Moreover, the hearts of *Srsf5*$^{-/-}$ mice showed mRNA overexpression of the myofibril fiber genes *Myh8*, *Neb*, and *Mylpf* (Figure 5F). This enrichment analysis suggested that *Srsf5* deficiency obstructed the cardiac function-specific transcriptome in the developmental heart.

Srsf5 is the splicing regulator of Myom1 in the perinatal heart

To identify the downstream targets of Srsf5, we subjected five Srsf5-dependent exons from five different genes (*Myom1*, *Col4a3bp*, *Ap1b1*, *Tgfb2*, and *Cnot2*) enriched in cardiac diseases to a more detailed RT-PCR analysis. We observed a reduction in exon skipping and exon inclusion in the hearts of *Srsf5* mutants, which is consistent with the previously reported function of SR proteins in the promotion of exon inclusion and the induction of exon skipping (Figure 6A) (Zhou and Fu, 2013). In the absence of Srsf5, the *Myom1* and *Ap1b1* transcripts containing the specified exons were found to increase, and *Col4a3bp*, *Tgfb2*, and *Cnot2* transcripts, in which exon skipping occurred, also increased. Among these, the exon skipping of *Myom1* around the time of birth has been extensively reported in the literature. MYOM1 is an essential component of sarcomeres (Grove et al., 1984). Exon 18 of *Myom1* is present in the Myom1 isoform of the avian and mammalian embryonic hearts, named EH-myomesin, which is rapidly excluded after birth to form the mature isoform (Agarkova et al., 2000). We found that exon 18 was unable to complete postnatal deletion in the absence of Srsf5 (Figure 6A). Myom1 protein expression in the hearts of WT and *Srsf5*$^{-/-}$ mice

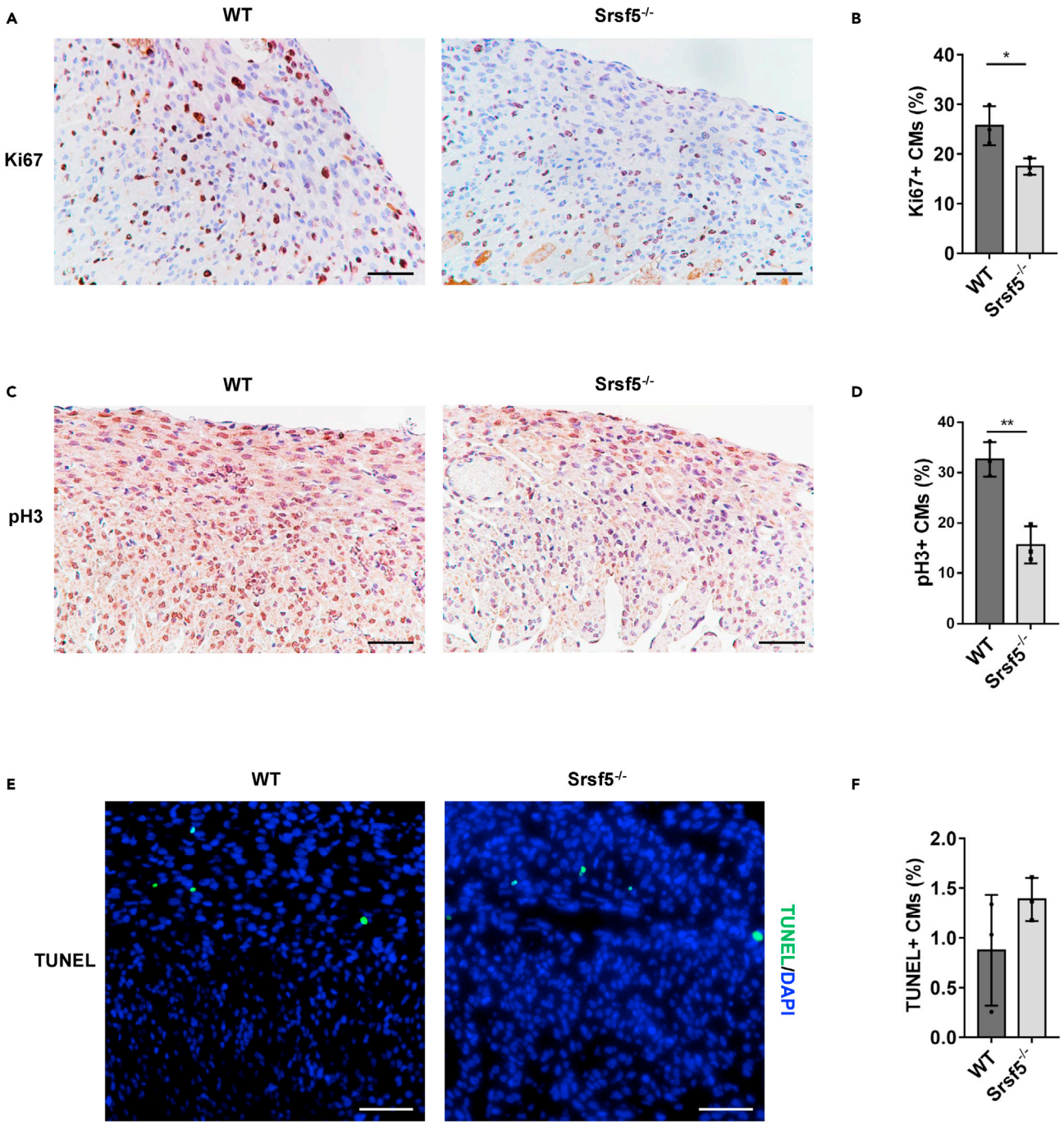

Figure 4. *Srsf5* deficiency represses cardiomyocyte proliferation

(A and B) Representative image of Ki67 immunohistochemical staining (A) and analysis of positive rates (B) at P1 hearts. Scale bar, 50 μm.

(C and D) Representative image of pH3 immunohistochemical staining (C) and analysis of positive rates (D) at P1 hearts. To analyze the positive rate of Ki67 and pH3 staining, five regions of each LV wall were randomly selected for counting and averaged. Scale bar, 50 μm.

(E) TUNEL (TdT-mediated dUTP nick-end labeling) fluorescence staining was used to analyze apoptosis in the hearts at P1. Scale bar, 50 μm.

(F) Quantification of TUNEL-positive cardiomyocytes (CMs). Data are represented as mean ± SD. *: $p< 0.05$, **: $p< 0.01$, Student's t-test.

from E13.5 to P1 was analyzed by western blotting (Figure 6B). The expression of the EH-myomesin isoform in the hearts of WT mice was significantly reduced after birth, whereas Myom1 expressed in the hearts of *Srsf5*$^{-/-}$ mice was dominated by the EH-myomesin isoform both at the embryonic and postnatal stage. To

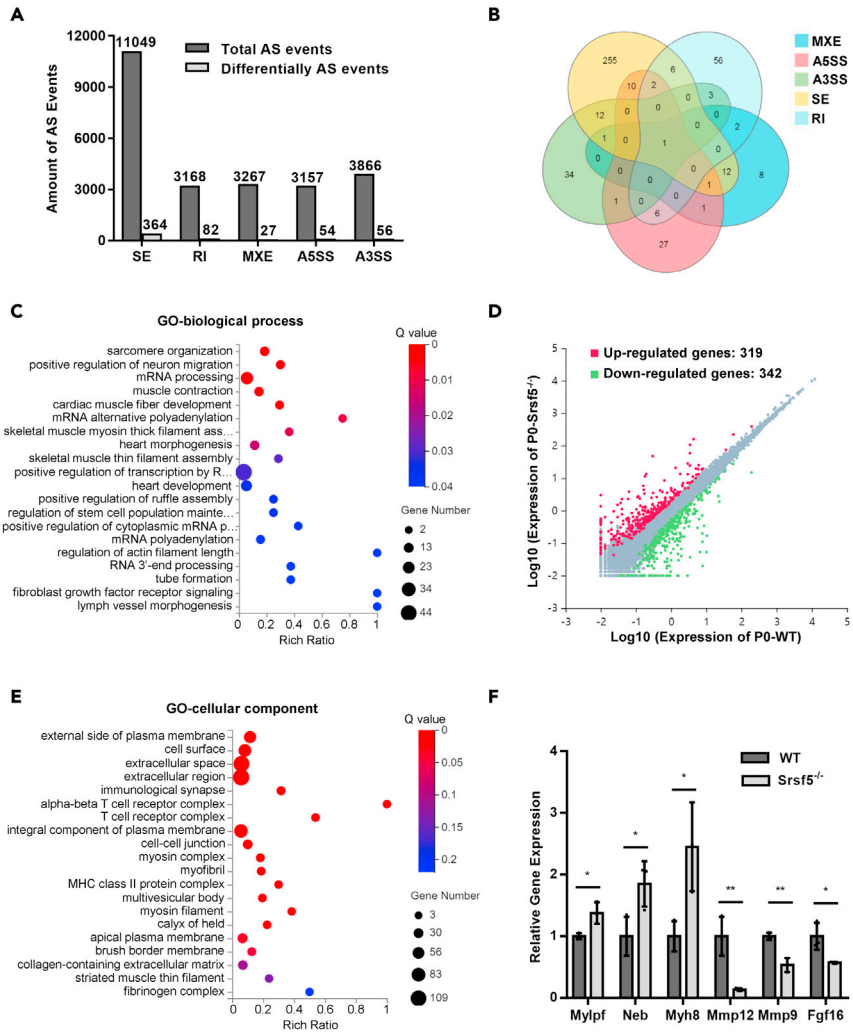

Figure 5. Srsf5 depletion alters the transcriptome and alternative splicing events in neonatal mice hearts

(A) Differentially alternative splicing (AS) patterns in the hearts of *Srsf5*$^{-/-}$ vs. WT mice at P0.

(B) Overlap of five types of AS genes illustrated in five-way Venn diagrams of the hearts of *Srsf5*$^{-/-}$ vs. WT mice at P0. The criteria for identifying significant splice differences were: absolute value of splice percentage at cutoff $\geq$0.20 and False Discovery Rates (FDR) $\leq$ 0.001.

(C) DAVID GO enrichment analysis of differentially spliced genes on biological processes.

(D) A scatter plot for all the differentially expressed genes with |log2FC| $\geq$ 1 and Q-value $\leq$ 0.001 in the hearts of *Srsf5*$^{-/-}$ vs. WT mice at P0.

(E) Detailed GO enrichment analysis of differentially expressed genes on cellular components.

(F) qRT-PCR validation of mRNA expression of genes regarding cell proliferation and constituents of sarcomeres in the hearts of WT and *Srsf5*$^{-/-}$ mice at P1. Data are represented as mean $\pm$ SD. *: p< 0.05, **: p< 0.01, Student's t-test.

See also Tables S4, S5, and S6.

further determine whether Srsf5 binds *Myom1* pre-mRNA directly *in vivo*, we conducted a nuclear RNA-binding protein immunoprecipitation (RIP) assay, and found that Srsf5 specifically bound to *Myom1* pre-mRNA (Figure 6C).

Furthermore, we generated a minigene construct containing exons 17 to 19 together with the two introns, based on the genomic region of mouse *Myom1* (Figure 6D). Co-transfection of the *Myc-Srsf5* and *Myom1* minigene into HEK293T cells revealed that the higher the Srsf5 expression, the more alternative exon 18 was excluded (Figure 6E). The minigene assay confirmed the regulation of *Myom1* splicing by Srsf5 in cells. From these results, we concluded that Srsf5 depletion in the heart was largely responsible for the defect in Myom1 alternative splicing.

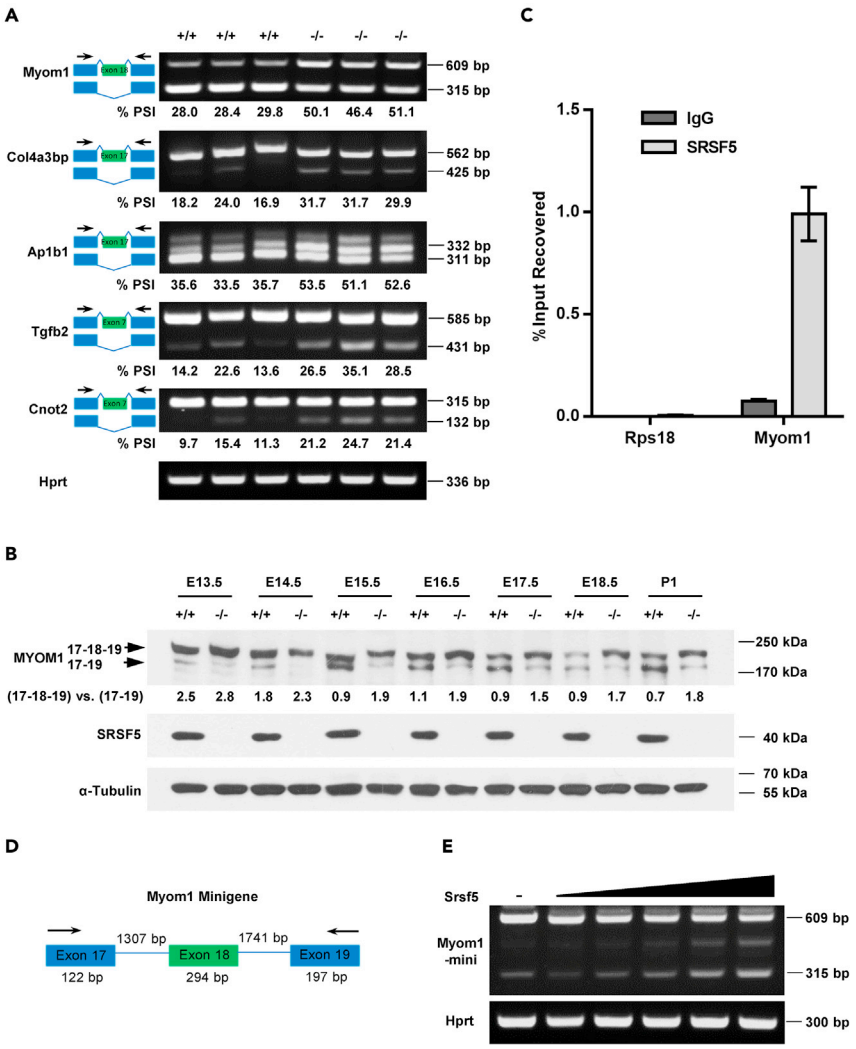

Figure 6. Srsf5 is the splicing regulator of Myom1 in the perinatal heart

(A) RT-PCR analysis of Srsf5-dependent splicing in P1 hearts. The black arrows show primer positions. The green rectangles represent Srsf5-dependent exons. %PSI (percentage splicing index) was calculated by dividing the included exon by both isoforms (*Myom1* and *Ap1b1*), or the excluded exon by both isoforms (*Col4a3bp*, *Tgfb2*, and *Cnot2*). *Hprt* was used as an internal reference. Thirty PCR cycles were performed, and all bands were verified by sequencing.

(B)Western blot analysis of Myom1 isoform switch in the hearts of WT and *Srsf5*$^{-/-}$ mice at different developmental stages. Myom1 in the hearts of *Srsf5*$^{-/-}$ mice was unable to complete the isoform switch. Isoform ratio between (17-18-19) and (17–19), indicating the inclusion of exon 18, was calculated and illustrated at the bottom.

(C) RIP assay was performed to detect the interaction of Srsf5 with *Myom1* pre-mRNA and *Rps18*was used as a negative control.

(D) Schematic diagram of the mouse *Myom1* minigene. Rectangles represent exons, horizontal lines represent introns, exon 18 is the alternative exon, and exon 17 and 19 are constitutive exons. The lengths (base pair) of exons and introns were shown. The black arrows represent the positions of the primer pairs used to detect the minigene.

(E) Effect of different doses of Srsf5 on *Myom1* minigene splicing. *Myc-Srsf5* (0, 250 ng, 500 ng, 1000 ng, 1500 ng, and 2000 ng) was co-transfected with *Myom1* minigene plasmid (250 ng) into 293T cells in 12-well plates. RNA was collected after 24 h for detection by RT-PCR.

DISCUSSION

Alternative splicing is a major step in pre-mRNA processing, ensuring the proper gene expression and diversification of human transcriptomes, and plays an important functional role during tissue and organ development (Baralle and Giudice, 2017; Nilsen and Graveley, 2010). The SR family of splicing factors plays a crucial role in mRNA splicing activation, repression, export, stabilization, and translation (Geuens et al.,

2016). Among the classical SR splicing factors, SRSF1, SRSF2, SRSF3, and SRSF10 have been reported to be indispensable for tissue development and the maintenance of function (Feng et al., 2009; Ortiz-Sánchez et al., 2019; Xu et al., 2005). As a member of SR-splicing factors, SRSF5 has been previously demonstrated to be involved in glucose metabolism and carcinogenesis by promoting the alterative splicing of PKCβII or CCAR1 (Chen et al., 2018; Patel et al., 2005). Here, we found that the systemic loss of Srsf5 caused perinatal death in mice, revealing a previously unrecognized functional role of Srsf5 in tissue development.

Furthermore, we revealed that Srsf5 depletion in mice resulted in cardiac dysfunction with noncompaction of the ventricular myocardium. During embryonic cardiomorphogenesis, coordinated compaction of the inner trabecular layer and growth of the outer layer of the myocardium are essential for the maturation of the ventricular wall (Sedmera et al., 2000). Arrested trabecular development is involved in the pathogenesis of hypertrabeculation associated with ventricular noncompaction cardiomyopathy (Zhang et al., 2013). Noncompaction cardiomyopathy (NCCM) is a rare cardiomyopathy characterized by abnormal ventricular myocardial protrusions with a thin layer of properly compacted myocardium, also known as left ventricular noncompaction cardiomyopathy (Choquet et al., 2018). NCCM has been described as a genetic disorder associated, with mutations in genes encoding cytoskeletal, ionic channels, and chaperone proteins (Klaassen et al., 2008; Towbin, 2014). *MYH7*, *MYBPC3*, and *TTN* mutations are the most frequent mutations (71%) found in the genetic NCCM (van Waning et al., 2018). A recent study reported that the deletion of the cardiac transcription factor Nkx2-5 during trabecular development resulted in pathological features associated with NCCM in adult mice (Choquet et al., 2018). NKX2-5 mutations have been identified in NCCM patients, suggesting that this transcription factor plays a role in compaction (Ashraf et al., 2014). Additionally, variants of the splicing factor RBM20 have been identified in patients with NCCM, and this pathogenic variant in RBM20 has been associated with worse clinical outcomes (Sedaghat-Hamedani et al., 2017). In this study, the functional role of the classical splicing factor Srsf5 was demonstrated, and *Srsf5* deficiency was found to disrupt the normal structure of the heart, resulting in cardiomyopathy with noncompaction of the ventricular myocardium.

However, we did not demonstrate whether cardiac dysfunction in *Srsf5*-deficiency mice is responsible for postnatal death. To address this issue, the conditional knockout of *Srsf5* in the mouse myocardium should be generated and analyzed in future studies. Additionally, it would be worthwhile to identify SRSF5 variants in patients with NCCM to determine the relationship between RNA splicing regulated by SRSF5 and NCCM disease.

Mechanistically, we found that Srsf5 promoted the alterative splicing of *Myom1*, which encodes myomesin-1 protein (Grove et al., 1984). MYOM1 consists of 13 motifs, including a unique N-terminal domain, followed by seven Ig-like and five Fn-like motifs (Steiner et al., 1998). MYOM1 acts as a structural linker in the sarcomere M-line, connecting with muscle-type creatine kinase (MCK), Titin, and Obscurin (Pernigo et al., 2017; Pinotsis et al., 2008). Myocardial atrophy has been observed in MYOM1-deficient embryonic stem cells, indicating that it plays an important role in the assembly of myofibrils (Hang et al., 2021). EH-myomesin, the splice isoform of myomesin-1, generated by the inclusion of an elastic segment in the center of the molecule, is the main M-band component in the embryonic heart of vertebrates (Agarkova et al., 2000). In 2011, Schoenauer et al. reported that EH-myomesin was upregulated in dilated hearts and may serve as a marker for DCM (Schoenauer et al., 2011), while MBNL family proteins have been found to act as *trans*-acting factors in the alternative splicing of *Myom1* exon 17a in mouse and human skeletal muscle (Koebis et al., 2011). In the present study, the results obtained from RNA-Seq and splicing assays using a *Myom1* minigene system indicated that Srsf5 is a key regulator of Myom1 alternative splicing. We found that exon 18 was unable to complete postnatal deletion in the absence of Srsf5. Furthermore, western blot analysis revealed that EH-myomesin isoforms were dominant in the hearts of P1 *Srsf5*$^{-/-}$ mice compared to the hearts of WT mice. Additionally, the RIP assay showed that Srsf5 binds to *Myom1* mRNA directly in heart tissue in mice. Thus, we identified an essential regulator of Myom1 alternative splicing and heart development. However, in the present study we have no data to support that Srsf5-dependent splicing of *Myom1* transcript is causative of the cardiac phenotype and responsible of the early perinatal lethality of *Srsf5*$^{-/-}$ mice, although Myom1 alternative splicing was defective in the absence of Srsf5.

To conclude, using a systemic knockout mouse model, we found that *Srsf5* deficiency resulted in perinatal lethality and cardiac dysfunction with noncompaction of the ventricular myocardium. Mechanistically, Srsf5 directly binds to *Myom1* pre-mRNA and promotes its alterative splicing in heart tissue. Therefore, Srsf5-regulated alternative splicing plays a critical role in heart development.

Limitations of the study

In this study, we identified Srsf5 as a regulator of Myom1 alternative splicing and heart development. It is with regret that at present there is no data for supporting Srsf5-dependent splicing of *Myom1* transcript as the immediate cause for the cardiac phenotype and the early perinatal lethality of *Srsf5*$^{-/-}$ mice, although Myom1 alternative splicing was defective in the absence of Srsf5.

STAR★METHODS

Detailed methods are provided in the online version of this paper and include the following:

- KEY RESOURCES TABLE
- RESOURCE AVAILABILITY
  - Lead contact
  - Materials availability
  - Data and code availability
- EXPERIMENTAL MODEL AND SUBJECT DETAILS
- METHOD DETAILS
  - RT-PCR and quantitative real-time PCR
  - Western blot analysis
  - Histology, immunohistochemistry, and immunofluorescence analysis
  - Neonatal echocardiography and electrocardiography
  - RNA-binding protein immunoprecipitation assay
  - RNA-sequencing analysis
- QUANTIFICATION AND STATISTICAL ANALYSIS

SUPPLEMENTAL INFORMATION

Supplemental information can be found online at https://doi.org/10.1016/j.isci.2021.103097.

ACKNOWLEDGMENTS

This work was supported by the general project of National Natural Science Foundation of China (NSFC) (grant number 31471326).

AUTHOR CONTRIBUTIONS

The project was conceived by C.P.C and L.Z. The experiments were designed by X.Z., Z.W., Q.X., Y.C. and W.L. Most of the experiments were established by X.Z. and Z.W. The *Srsf5*$^{-/-}$ mice were generated by X.Z., Y.C. and W.L. The phenotype of *Srsf5*$^{-/-}$ mice was analyzed by X.Z., Z.W. and Q.X. PCR assays were performed by T.Z. and H.L. The data were analyzed by C.P.C., L.Z and C.Q. The manuscript was written by C.P.C., L.Z. and C.Q.

DECLARATION OF INTERESTS

The authors have no conflicts of interest to declare.

Received: April 9, 2021
Revised: July 17, 2021
Accepted: September 6, 2021
Published: October 22, 2021

REFERENCES

Agarkova, I., Auerbach, D., Ehler, E., and Perriard, J.C. (2000). A novel marker for vertebrate embryonic heart, the EH-myomesin isoform. J. Biol. Chem. *275*, 10256–10264. https://doi.org/10.1074/jbc.275.14.10256.

Ashraf, H., Pradhan, L., Chang, E.I., Terada, R., Ryan, N.J., Briggs, L.E., Chowdhury, R., Zárate, M.A., Sugi, Y., Nam, H.J., et al. (2014). A mouse model of human congenital heart disease: high incidence of diverse cardiac anomalies and ventricular noncompaction produced by heterozygous Nkx2-5 homeodomain missense mutation. Circ. Cardiovasc. Genet. *7*, 423–433. https://doi.org/10.1161/circgenetics.113.000281.

Baralle, F.E., and Giudice, J. (2017). Alternative splicing as a regulator of development and tissue identity. Nat. Rev. Mol. Cell Biol. *18*, 437–451. https://doi.org/10.1038/nrm.2017.27.

Barbosa-Morais, N.L., Irimia, M., Pan, Q., Xiong, H.Y., Gueroussov, S., Lee, L.J., Slobodeniuc, V., Kutter, C., Watt, S., Colak, R., et al. (2012). The evolutionary landscape of alternative splicing in vertebrate species. Science *338*, 1587–1593. https://doi.org/10.1126/science.1230612.

Botti, V., McNicoll, F., Steiner, M.C., Richter, F.M., Solovyeva, A., Wegener, M., Schwich, O.D., Poser, I., Zarnack, K., Wittig, I., et al. (2017).

Cellular differentiation state modulates the mRNA export activity of SR proteins. J. Cell Biol. *216*, 1993–2009. https://doi.org/10.1083/jcb.201610051.

Buratti, E., Stuani, C., De Prato, G., and Baralle, F.E. (2007). SR protein-mediated inhibition of CFTR exon 9 inclusion: molecular characterization of the intronic splicing silencer. Nucleic Acids Res. *35*, 4359–4368. https://doi.org/10.1093/nar/gkm444.

Chen, Y., Huang, Q., Liu, W., Zhu, Q., Cui, C.P., Xu, L., Guo, X., Wang, P., Liu, J., Dong, G., et al. (2018). Mutually exclusive acetylation and ubiquitylation of the splicing factor SRSF5 control tumor growth. Nat. Commun. *9*, 2464. https://doi.org/10.1038/s41467-018-04815-3.

Cheng, Y., Luo, C., Wu, W., Xie, Z., Fu, X., and Feng, Y. (2016). Liver-specific deletion of SRSF2 caused acute liver failure and early death in mice. Mol. Cell.Biol. *36*, 1628–1638. https://doi.org/10.1128/mcb.01071-15.

Choquet, C., Nguyen, T.H.M., Sicard, P., Buttigieg, E., Tran, T.T., Kober, F., Varlet, I., Sturny, R., Costa, M.W., Harvey, R.P., et al. (2018). Deletion of Nkx2-5 in trabecular myocardium reveals the developmental origins of pathological heterogeneity associated with ventricular non-compaction cardiomyopathy. PLoS Genet. *14*, e1007502. https://doi.org/10.1371/journal.pgen.1007502.

Crick, F. (1979). Split genes and RNA splicing. Science *204*, 264–271. https://doi.org/10.1126/science.373120.

D'Amato, G., Luxan, G., del Monte-Nieto, G., Martinez-Poveda, B., Torroja, C., Walter, W., Bochter, M.S., Benedito, R., Cole, S., Martinez, F., et al. (2016). Sequential Notch activation regulates ventricular chamber development. Nat. Cell Biol. *18*, 7–20. https://doi.org/10.1038/ncb3280.

Diamond, R.H., Du, K., Lee, V.M., Mohn, K.L., Haber, B.A., Tewari, D.S., and Taub, R. (1993). Novel delayed-early and highly insulin-induced growth response genes.Identification of HRS, a potential regulator of alternative pre-mRNA splicing. J. Biol. Chem. *268*, 15185–15192.

Du, K., Peng, Y., Greenbaum, L.E., Haber, B.A., and Taub, R. (1997). HRS/SRp40-mediated inclusion of the fibronectin EIIIB exon, a possible cause of increased EIIIB expression in proliferating liver. Mol. Cell.Biol. *17*, 4096–4104. https://doi.org/10.1128/mcb.17.7.4096.

Dwivedi, A., Slater, S.C., and George, S.J. (2009). MMP-9 and -12 cause N-cadherin shedding and thereby beta-catenin signalling and vascular smooth muscle cell proliferation. Cardiovasc.Res. *81*, 178–186. https://doi.org/10.1093/cvr/cvn278.

Feng, Y., Valley, M.T., Lazar, J., Yang, A.L., Bronson, R.T., Firestein, S., Coetzee, W.A., and Manley, J.L. (2009). SRp38 regulates alternative splicing and is required for Ca(2+) handling in the embryonic heart. Dev. Cell. *16*, 528–538. https://doi.org/10.1016/j.devcel.2009.02.009.

Fu, X.D., and Ares, M., Jr. (2014). Context-dependent control of alternative splicing by RNA-binding proteins. Nat. Rev. Genet. *15*, 689–701. https://doi.org/10.1038/nrg3778.

Galdos, F.X., Guo, Y., Paige, S.L., VanDusen, N.J., Wu, S.M., and Pu, W.T. (2017). Cardiac regeneration: lessons from development. Circ. Res. *120*, 941–959. https://doi.org/10.1161/CIRCRESAHA.116.309040.

Geuens, T., Bouhy, D., and Timmerman, V. (2016). The hnRNP family: insights into their role in health and disease. Hum. Genet. *135*, 851–867. https://doi.org/10.1007/s00439-016-1683-5.

Grove, B.K., Kurer, V., Lehner, C., Doetschman, T.C., Perriard, J.C., and Eppenberger, H.M. (1984). A new 185,000-dalton skeletal muscle protein detected by monoclonal antibodies. J. Cell Biol. *98*, 518–524. https://doi.org/10.1083/jcb.98.2.518.

Hang, C., Song, Y., Li, Y., Zhang, S., Chang, Y., Bai, R., Saleem, A., Jiang, M., Lu, W., Lan, F., et al. (2021). Knockout of MYOM1 in human cardiomyocytes leads to myocardial atrophy via impairing calcium homeostasis. J. Cell.Mol. Med. *25*, 1661–1676. https://doi.org/10.1111/jcmm.16268.

Ichida, F. (2020). Left ventricular noncompaction - risk stratification and genetic consideration. J. Cardiol. *75*, 1–9. https://doi.org/10.1016/j.jjcc.2019.09.011.

Kim, M.S., Pinto, S.M., Getnet, D., Nirujogi, R.S., Manda, S.S., Chaerkady, R., Madugundu, A.K., Kelkar, D.S., Isserlin, R., Jain, S., et al. (2014). A draft map of the human proteome. Nature *509*, 575–581. https://doi.org/10.1038/nature13302.

Klaassen, S., Probst, S., Oechslin, E., Gerull, B., Krings, G., Schuler, P., Greutmann, M., Hurlimann, D., Yegitbasi, M., Pons, L., et al. (2008). Mutations in sarcomere protein genes in left ventricular noncompaction. Circulation *117*, 2893–2901. https://doi.org/10.1161/CIRCULATIONAHA.107.746164.

Koebis, M., Ohsawa, N., Kino, Y., Sasagawa, N., Nishino, I., and Ishiura, S. (2011). Alternative splicing of myomesin 1 gene is aberrantly regulated in myotonic dystrophy type 1. Genes Cells *16*, 961–972. https://doi.org/10.1111/j.1365-2443.2011.01542.x.

Kuo, B.A., Uporova, T.M., Liang, H., Bennett, V.D., Tuan, R.S., and Norton, P.A. (2002). Alternative splicing during chondrogenesis: modulation of fibronectin exon EIIIA splicing by SR proteins. J. Cell.Biochem. *86*, 45–55. https://doi.org/10.1002/jcb.10188.

Lavine, K.J., Yu, K., White, A.C., Zhang, X., Smith, C., Partanen, J., and Ornitz, D.M. (2005). Endocardial and epicardial derived FGF signals regulate myocardial proliferation and differentiation in vivo. Dev. Cell. *8*, 85–95. https://doi.org/10.1016/j.devcel.2004.12.002.

Lee, Y., and Rio, D.C. (2015). Mechanisms and regulation of alternative pre-mRNA splicing. Annu. Rev. Biochem. *84*, 291–323. https://doi.org/10.1146/annurev-biochem-060614-034316.

Love, M.I., Huber, W., and Anders, S. (2014). Moderated estimation of fold change and dispersion for RNA-seq data with DESeq2. Genome Biol. *15*, 550. https://doi.org/10.1186/s13059-014-0550-8.

Lu, C., Li, J.Y., Ge, Z., Zhang, L., and Zhou, G.P. (2013). Par-4/THAP1 complex and Notch3 competitively regulated pre-mRNA splicing of CCAR1 and affected inversely the survival of T-cell acute lymphoblastic leukemia cells. Oncogene *32*, 5602–5613. https://doi.org/10.1038/onc.2013.349.

Maron, B.J., Towbin, J.A., Thiene, G., Antzelevitch, C., Corrado, D., Arnett, D., Moss, A.J., Seidman, C.E., and Young, J.B. (2006). Contemporary definitions and classification of the cardiomyopathies: an American heart association scientific statement from the council on clinical cardiology, heart failure and transplantation committee; quality of Care and outcomes Research and functional genomics and translational biology interdisciplinary working groups; and council on epidemiology and prevention. Circulation *113*, 1807–1816. https://doi.org/10.1161/circulationaha.106.174287.

Merkin, J., Russell, C., Chen, P., and Burge, C.B. (2012). Evolutionary dynamics of gene and isoform regulation in mammalian tissues. Science *338*, 1593–1599. https://doi.org/10.1126/science.1228186.

Mitchell, G.F., Jeron, A., and Koren, G. (1998). Measurement of heart rate and Q-T interval in the conscious mouse. Am. J. Physiol. *274*, H747–H751. https://doi.org/10.1152/ajpheart.1998.274.3.H747.

Nilsen, T.W., and Graveley, B.R. (2010). Expansion of the eukaryotic proteome by alternative splicing. Nature *463*, 457–463. https://doi.org/10.1038/nature08909.

Ortiz-Sánchez, P., Villalba-Orero, M., López-Olañeta, M.M., Larrasa-Alonso, J., Sánchez-Cabo, F., Martí-Gómez, C., Camafeita, E., Gómez-Salinero, J.M., Ramos-Hernández, L., Nielsen, P.J., et al. (2019). Loss of SRSF3 in cardiomyocytes leads to decapping of contraction-related mRNAs and severe systolic dysfunction. Circ. Res. *125*, 170–183. https://doi.org/10.1161/circresaha.118.314515.

Patel, N.A., Kaneko, S., Apostolatos, H.S., Bae, S.S., Watson, J.E., Davidowitz, K., Chappell, D.S., Birnbaum, M.J., Cheng, J.Q., and Cooper, D.R. (2005). Molecular and genetic studies imply Akt-mediated signaling promotes protein kinase CbetaII alternative splicing via phosphorylation of serine/arginine-rich splicing factor SRp40. J. Biol. Chem. *280*, 14302–14309. https://doi.org/10.1074/jbc.M411485200.

Pernigo, S., Fukuzawa, A., Beedle, A.E.M., Holt, M., Round, A., Pandini, A., Garcia-Manyes, S., Gautel, M., and Steiner, R.A. (2017). Binding of myomesin to obscurin-like-1 at the muscle M-band provides a strategy for isoform-specific mechanical protection. Structure *25*, 107–120. https://doi.org/10.1016/j.str.2016.11.015.

Pinotsis, N., Lange, S., Perriard, J.C., Svergun, D.I., and Wilmanns, M. (2008). Molecular basis of the C-terminal tail-to-tail assembly of the sarcomeric filament protein myomesin. EMBO J. *27*, 253–264. https://doi.org/10.1038/sj.emboj.7601944.

Schoenauer, R., Emmert, M.Y., Felley, A., Ehler, E., Brokopp, C., Weber, B., Nemir, M., Faggian, G.G., Pedrazzini, T., Falk, V., et al. (2011). EH-myomesin splice isoform is a novel marker for dilated cardiomyopathy. Basic Res. Cardiol. *106*, 233–247. https://doi.org/10.1007/s00395-010-0131-2.

Sebbag-Sznajder, N., Raitskin, O., Angenitzki, M., Sato, T.A., Sperling, J., and Sperling, R. (2012). Regulation of alternative splicing within the supraspliceosome. J. Struct. Biol. *177*, 152–159. https://doi.org/10.1016/j.jsb.2011.11.005.

Sedaghat-Hamedani, F., Haas, J., Zhu, F., Geier, C., Kayvanpour, E., Liss, M., Lai, A., Frese, K., Pribe-Wolferts, R., Amr, A., et al. (2017). Clinical genetics and outcome of left ventricular non-compaction cardiomyopathy. Eur. Heart J. *38*, 3449–3460. https://doi.org/10.1093/eurheartj/ehx545.

Sedmera, D., Pexieder, T., Vuillemin, M., Thompson, R.P., and Anderson, R.H. (2000). Developmental patterning of the myocardium. Anat. Rec. *258*, 319–337. https://doi.org/10.1002/(sici)1097-0185(20000401)258:4<319::Aid-ar1>3.0.Co;2-o.

Sharp, P.A. (1994). Split genes and RNA splicing. Cell *77*, 805–815. https://doi.org/10.1016/0092-8674(94)90130-9.

Shen, S., Park, J.W., Lu, Z.X., Lin, L., Henry, M.D., Wu, Y.N., Zhou, Q., and Xing, Y. (2014). rMATS: robust and flexible detection of differential alternative splicing from replicate RNA-Seq data. Proc. Natl. Acad. Sci. U S A *111*, E5593–E5601. https://doi.org/10.1073/pnas.1419161111.

Shepard, P.J., and Hertel, K.J. (2009). The SR protein family. Genome Biol. *10*, 242. https://doi.org/10.1186/gb-2009-10-10-242.

Shi, Y. (2017). Mechanistic insights into precursor messenger RNA splicing by the spliceosome. Nat. Rev. Mol. Cell.Biol. *18*, 655–670. https://doi.org/10.1038/nrm.2017.86.

Steiner, F., Weber, K., and Fürst, D.O. (1998). Structure and expression of the gene encoding murine M-protein, a sarcomere-specific member of the immunoglobulin superfamily. Genomics *49*, 83–95. https://doi.org/10.1006/geno.1998.5220.

Towbin, J.A. (2014). Ion channel dysfunction associated with arrhythmia, ventricular noncompaction, and mitral valve prolapse: a new overlapping phenotype. J. Am. Coll. Cardiol. *64*, 768–771. https://doi.org/10.1016/j.jacc.2014.06.1154.

van den Hoogenhof, M.M.G., Pinto, Y.M., and Creemers, E.E. (2016). RNA splicing. Circ. Res. *118*, 454–468. https://doi.org/10.1161/circresaha.115.307872.

van Waning, J.I., Caliskan, K., Hoedemaekers, Y.M., van Spaendonck-Zwarts, K.Y., Baas, A.F., Boekholdt, S.M., van Melle, J.P., Teske, A.J., Asselbergs, F.W., Backx, A., et al. (2018). Genetics, clinical features, and long-term outcome of noncompaction cardiomyopathy. J. Am. Coll. Cardiol. *71*, 711–722. https://doi.org/10.1016/j.jacc.2017.12.019.

Wang, H.Y., Xu, X., Ding, J.H., Bermingham, J.R., Jr., and Fu, X.D. (2001). SC35 plays a role in T cell development and alternative splicing of CD45. Mol. Cell. *7*, 331–342. https://doi.org/10.1016/s1097-2765(01)00181-2.

Wilsbacher, L., and McNally, E.M. (2016). Genetics of cardiac developmental disorders: cardiomyocyte proliferation and growth and relevance to heart failure. Annu. Rev. Pathol. *11*, 395–419. https://doi.org/10.1146/annurev-pathol-012615-044336.

Wu, P., Geng, B., Chen, Q., Zhao, E., Liu, J., Sun, C., Zha, C., Shao, Y., You, B., Zhang, W., et al. (2020). Tumor cell-derived TGFbeta1 attenuates antitumor immune activity of T cells via regulation of PD-1 mRNA. Cancer Immunol.Res. *8*, 1470–1484. https://doi.org/10.1158/2326-6066.CIR-20-0113.

Xu, X., Yang, D., Ding, J.H., Wang, W., Chu, P.H., Dalton, N.D., Wang, H.Y., Bermingham, J.R., Jr., Ye, Z., Liu, F., et al. (2005). ASF/SF2-regulated CaMKIIdelta alternative splicing temporally reprograms excitation-contraction coupling in cardiac muscle. Cell *120*, 59–72. https://doi.org/10.1016/j.cell.2004.11.036.

Zhang, W., Chen, H., Qu, X., Chang, C.P., and Shou, W. (2013). Molecular mechanism of ventricular trabeculation/compaction and the pathogenesis of the left ventricular noncompaction cardiomyopathy (LVNC). Am. J. Med. Genet. C Semin. Med. Genet. *163c*, 144–156. https://doi.org/10.1002/ajmg.c.31369.

Zhou, Z., and Fu, X.D. (2013). Regulation of splicing by SR proteins and SR protein-specific kinases. Chromosoma *122*, 191–207. https://doi.org/10.1007/s00412-013-0407-z.

Zou, J., Ma, W., Li, J., Littlejohn, R., Zhou, H., Kim, I.M., Fulton, D.J.R., Chen, W., Weintraub, N.L., Zhou, J., et al. (2018). Neddylation mediates ventricular chamber maturation through repression of Hippo signaling. Proc. Natl. Acad. Sci. U S A *115*, E4101–E4110. https://doi.org/10.1073/pnas.1719309115.

STAR★METHODS

KEY RESOURCES TABLE

REAGENT or RESOURCE	SOURCE	IDENTIFIER
Antibodies		
anti-SRSF5	MBL	Cat#RN082PW; RRID:AB_11160960
anti-MYOM1	Proteintech	Cat#20360-1-AP; RRID:AB_2878989
α-Tubulin	Proteintech	Cat#66031-1-Ig; RRID:AB_11042766
anti-SRSF5	Sigma-Aldrich	Cat#HPA043484; RRID:AB_10797143
anti-Ki67	CST	Cat#9449S; RRID:AB_2797703
anti-pH3	Immunoway	Cat#YP0129
anti-cTnT	DSHB	Cat#CT3; RRID:AB_528495
anti-Endomucin	Santa Cruz Biotechnology	Cat#sc-65495; RRID:AB_2100037
HRP-conjugated anti-mouse secondary antibody	Jackson ImmunoResearch	Cat#115-035-003, RRID:AB_10015289
HRP-conjugated anti-rabbit secondary antibody	Jackson ImmunoResearch	Cat#111-035-008, RRID:AB_2337937
Chemicals, peptides, and recombinant proteins		
Protease inhibitor cocktail	MCE	Cat#HY-K0010
TRIzol reagent	Invitrogen	Cat#15596018
Critical commercial assays		
Reverse transcription kit	TOYOBO	Cat#FSQ-201
Rabbit two-step assay kit	ZSGB-BIO	Cat#PV-9001
EZ-Nuclear RIP (Cross-Linked) kit	Millipore	Cat#17-10521
Deposited data		
Raw and Analyzed sequence data	This paper	SRA: PRJNA708182 https://www.ncbi.nlm.nih.gov/sra/?term=PRJNA708182
Experimental models: Cell lines		
Human HEK293T	N/A	N/A
Experimental models: Organisms/strains		
Mus musculus: C57Bl/6J	Nanjing Biomedical Research Institute of Nanjing University	Cat# XM003240
Oligonucleotides		
Primers for RT-PCR and qRT-PCR, see Table S3	This paper	N/A
Software and algorithms		
Prism7	Graphpad	https://www.graphpad.com/scientific-software/prism/

RESOURCE AVAILABILITY

Lead contact

Further information and requests for resources and reagents should be directed to and will be fulfilled by the lead contact, Chun-Ping Cui (cui_chunping2000@aliyun.com).

Materials availability

This study did not generate new unique reagents.

Data and code availability

- RNA sequencing data have been deposited in the Sequence Read Archive (SRA) and are publicly available as of the date of publication (https://www.ncbi.nlm.nih.gov/sra/?term=PRJNA708182). Accession numbers are listed in the key resources table. All data reported in this paper will be shared by the lead contact upon request.
- This paper does not report original code.
- Any additional information required to reanalyze the data reported in this paper is available from the lead contact upon request.

EXPERIMENTAL MODEL AND SUBJECT DETAILS

All animal experiments were approved by the Institutional Animal Care and Use Committee (IACUC) of the Beijing Institute of Lifeomics. Our experimental mice were housed in an animal barrier facility with temperature and humidity controlled at 25°C and 40–70%, respectively, with a light/dark cycle set at 12 h light/12 h dark. Both female and male mice at 10-16 weeks were used for breeding, and mice in embryonic and perinatal periods were mainly used for this study.

Srsf5$^{+/-}$ mice were purchased from Nanjing Biomedical Research Institute of Nanjing University. Two female and one male heterozygous mice were caged for breeding. The production of a vaginal plug the following morning indicated mating, which was denoted as 0.5 days of gestation. Male mice were removed to avoid mating recurrence. The mice used in our study were from C57/BL6J inbred backgrounds.

METHOD DETAILS

RT-PCR and quantitative real-time PCR

Total RNA was prepared using the TRIzol reagent (cat. no. 15596018; Invitrogen), according to the manufacturer's instructions. Total RNA was extracted from animal tissues or cell lines, and cDNA was prepared using a reverse transcription kit (FSQ-201; TOYOBO). The primers used for each gene are listed in Table S3. For RT-PCR, 25–30 cycles of PCR were performed with Golden Star T6 Super PCR Mix (Tsingke). Quantitative real-time PCR (qRT-PCR) was performed in a Roche LightCycler and the ΔΔCt method was used to analyze the data.

Western blot analysis

Tissues were homogenized with RIPA lysis buffer containing a protease inhibitor cocktail (1:100) (HY-K0010; MCE) and extracted for protein. Protein samples were separated by SDS-PAGE and electrotransferred onto nitrocellulose membranes. The primary antibodies used were as follows: anti-SRSF5 (1:10009 (RN082PW; MBL), anti-MYOM1 (1:500) (20360-1-AP; Proteintech), and α-tubulin (1:50000) (66031-1-Ig; Proteintech). HRP-conjugated secondary antibodies from Jackson ImmunoResearch were employed (1:3000) (anti-mouse IgG; 115-035-003) (anti-rabbit IgG; 111-035-008) and detected by SuperSignal West Pico PLUS Chemiluminescent Substrate (Thermo Fisher Scientific).

Histology, immunohistochemistry, and immunofluorescence analysis

All tissues were fixed in 4% paraformaldehyde, paraffin-embedded, and cut into 5-μm sections for subsequent staining. For histological analysis, paraffin sections were deparaffinized, hydrated, and stained with hematoxylin and eosin (H&E). For immunohistochemical analysis, the sections were incubated in prewarmed citrate buffer (pH 6.0) for 15 min in a low-heat microwave oven. After blocking with 10% goat serum (ZLI-9021; ZSGB-BIO) to prevent non-specific binding, the sections were incubated overnight at 4°C with primary antibodies against anti-SRSF5 (1:1500) (HPA043484; Sigma-Aldrich), anti-Ki67 (1:400) (9449S; CST), and anti-pH3 (1:500) (YP0129; Immunoway), respectively. Staining was completed using a rabbit two-step assay kit (PV-9001; ZSGB-BIO) according to the manufacturer's instructions. Images were acquired using Pannoramic MIDI 3D HISTECH.

Immunofluorescence staining was performed in the same way as histochemical staining prior to primary antibody incubation. The primary antibodies used were anti-cTnT (1:3) (CT3; DSHB) and anti-Endomucin (1:50) (sc-65495; Santa Cruz Biotechnology). Then, the slides were washed with PBS and incubated with the fluorescent secondary antibody for 1 h at room temperature. Fluorescence nuclear staining was performed using DAPI. Fluorescent images were acquired using Pannoramic MIDI of 3D HISTECH.

Neonatal echocardiography and electrocardiography

Echocardiography of P1 neonates was performed by gently fixing the limbs and heads of mice with tape on the station at a temperature of 25°C. Cardiac images were collected using a VEVO 2100 echocardiography imaging system and a 50 MHz transducer (Fujifilm Visual Sonics). The LV functional parameters were analyzed using VEVO 2100 software.

Electrocardiography was recorded using a digital electrocardiograph (BES307DT; BMV) modified with silver pin electrodes, and the data were analyzed using computer software. Corrected QT intervals were obtained using the formula $QT/(RR/100)^{1/2}$, as previously described (Mitchell et al., 1998). P1 neonates were secured using the same approach as that used for echocardiography.

RNA-binding protein immunoprecipitation assay

RNA-binding protein immunoprecipitation experiments were performed using an EZ-Nuclear RIP (Cross-Linked) kit (catalog no. 17-10521; Millipore) according to the manufacturer's instructions. Briefly, we validated the Srsf5 interaction with pre-mRNA using 100 mg of fresh heart tissue from 1-day-old mice. After cross-linking the protein and RNA/DNA using formaldehyde at a final concentration of 0.3%, the cross-linked products were released by lysing the cells. Cross-linked DNA was sheared to a length of approximately 200-1000 bp using a cell sonicator. After co-incubating the antibody with magnetic beads for 30 min at room temperature to form a complex, immunoprecipitation with RNA-binding protein-RNA complexes was performed. The antibody used for immunoprecipitation was anti-SRSF5 (1:100) (RN082PW; MBL). After the cross-linking reversal reaction, the protein was separated from the interacting RNA, and the RNA was purified for subsequent qRT-PCR. To obtain sufficient amounts of RNA after immunoprecipitation, the precipitation reactions shown in the instructions were performed at least in triplicate.

RNA-sequencing analysis

For RNA-seq, P0 wild-type and *Srsf5*$^{-/-}$ mouse hearts with three biological replicates each were subjected to total RNA extraction by the Beijing Genomic Institute (BGI) (www.genomics.org.cn) (Figure 5). RNA sequencing was also performed by BGI. Libraries were prepared using polyA+ selection, and sequencing was performed using a DNBSEQ platform, ensuring an average of 75 million paired-end reads per sample with 150 bp per read length (PE150). Differential expression analysis was performed using DESeq2 (v1.4.5) (Love et al., 2014) with a Q-value $\leq$ 0.05. GO analysis of differentially expressed genes was performed to gain insight into the phenotypic changes (http://www.geneontology.org/). BGI used rMATS (v3.2.5) (Shen et al., 2014) to detect differentially spliced genes between different samples and splicing events in the samples themselves. The reference genome sequenced was the NCBI version of GCF_000001635.26_GRCm38.p6 on mus-musculus. The original sequence data were submitted to the NCBI Sequence Read Archive database (https://trace.ncbi.nlm.nih.gov/Traces/sra) under accession number PRJNA708182.

QUANTIFICATION AND STATISTICAL ANALYSIS

GraphPad Prism 7 software was used for statistical analysis. Mice were grouped according to genotype, and Student's t-test was used to define the statistical significance of the differences between groups. $P< 0.05$ was considered significant. pvalues were shown on the figures as asterisks: *, $p< 0.05$; **, $p< 0.01$; ***, $p< 0.001$; ****, $p< 0.0001$. The data in the graphs are presented as mean $\pm$ SD. Independently performed biological replicates (n values) are indicated as dots in the bar graphs.